View metadata, citation and similar papers at core.ac.uk

brought to you by CORE

provided by University of Strathclyde Institutional Repository

Ricciardi, Lorenzo A. and Maddock, Christie Alisa and Vasile, Massimiliano (2018) Multi-objective optimal control of re-entry and abort scenarios. In: AIAA SciTech 2018, 2018-01-08 - 2018-01-12, Gaylord Palms. , http://dx.doi.org/10.2514/6.2018-0218

This version is available at https://strathprints.strath.ac.uk/63152/

Strathprints is designed to allow users to access the research output of the University of Strathclyde. Unless otherwise explicitly stated on the manuscript, Copyright © and Moral Rights for the papers on this site are retained by the individual authors and/or other copyright owners. Please check the manuscript for details of any other licences that may have been applied. You may not engage in further distribution of the material for any profitmaking activities or any commercial gain. You may freely distribute both the url (https://strathprints.strath.ac.uk/) and the content of this paper for research or private study, educational, or not-for-profit purposes without prior permission or charge.

Any correspondence concerning this service should be sent to the Strathprints administrator: strathprints@strath.ac.uk

The Strathprints institutional repository (https://strathprints.strath.ac.uk) is a digital archive of University of Strathclyde research outputs. It has been developed to disseminate open access research outputs, expose data about those outputs, and enable the management and persistent access to Strathclyde's intellectual output.

Multi-Objective Optimal Control of Re-entry and Abort Scenarios

Lorenzo A. Ricciardi*, Christie Alisa Maddock† and Massimiliano Vasile‡
University of Strathclyde, Glasgow, United Kingdom, G1 1XJ

This paper presents a novel approach to the solution of multi-phase multi-objective optimal control problems. The proposed solution strategy is based on the integration of the Direct Finite Elements Transcription (DFET) method, to transcribe dynamics and objectives, with a memetic strategy called Multi Agent Collaborative Search (MACS). The original multi-objective optimal control problem is reformulated as two non-linear programming problems: a bi-level and a single level one. In the bi-level problem the outer level, handled by MACS, generates trial control vectors that are then passed to the inner level, which enforces the feasibility of the solution. Feasible control vectors are then returned to the outer level to evaluate the corresponding objective functions. A single level refinement is then run to improve local convergence to the Pareto front. The paper introduces also a novel parameterisation of the controls, using Bernstein polynomials, in the context of the DFET transcription method. The approach is first tested on a known atmospheric re-entry problem and then applied to the analysis of ascent and abort trajectories for a space plane.

Nomenclature

α	Angle of attack
β	Bank angle
$\boldsymbol{\psi}$	Boundary constraints
ΔT	Length of element
δ_T	Throttle
γ	Flight path angle
λ	Longitude
$\mathbf{F}$	Differential equations of motion
$\mathbf{g}$	Algebraic constraints
$\mathbf{u}$	Control vector
$\mathbf{w}$	Weight function
$\mathbf{x}$	State vector
$\mathbf{x}_0$	Initial conditions
$\mathbf{x}_f$	Final conditions
μ_E	Gravitational parameter of Earth
ω_E	Magnitude of angular velocity of Earth
ψ	Azimuth angle
ρ	Atmospheric density
σ_k	Gauss integration weights
τ	Adimensional time
τ_k	Gauss integration nodes
θ	Latitude
A_e	Nozzle exit area
a_{max}	Magnitude of maximum admissible acceleration
C_D	Drag coefficient
C_L	Lift coefficient
D	Aerodynamic drag force
F_T	Magnitude of thrust
g	Magnitude of gravitational acceleration
g_0	Magnitude of gravitational acceleration at sea level
h	Altitude with respect to sea level
I_{sp}	Specific impulse

*Ph.D. Candidate, Aerospace Centre of Excellence, Mechanical & Aerospace Engineering, 75 Montrose Street, G1 1XJ, Glasgow, AIAA Student Member.
†Lecturer, Aerospace Centre of Excellence, Mechanical & Aerospace Engineering, 75 Montrose Street, G1 1XJ, Glasgow, AIAA Member.
‡Professor, Aerospace Centre of Excellence, Mechanical & Aerospace Engineering, 75 Montrose Street, G1 1XJ, Glasgow, AIAA Member.

J	Objective function(s)
L	Aerodynamic lift force
M	Mach number
m	Vehicle mass
N	Number of discretisation elements
P_a	Atmospheric pressure
P_e	Exhaust pressure at the nozzle
Q	Heat flux
Q_{max}	Maximum heat flux
q_{max}	Maximum dynamic pressure
R_E	Radius of Earth
t	Time
t_0	Initial time
t_f	Final time
T_{vac}	Modulus of thrust in vacuum
v	Velocity in inertial frame
$W_{L,max}$	Maximum wing loading
DFET	Direct Finite Elements in Time
ECEF	Earth Centred Earth Fixed reference frame
MACS	Multi Agent Collaborative Search
NLP	Non linear programming

I. Introduction

This paper proposes a method for the solution of multi-objective optimal control problems. The method is based on a direct transcription with Direct Finite Elements in Time [1] (DFET) and a solution of the resulting multi-objective nonlinear programming (NLP) problem with a version of Multi Agent Collaborative Search [2] (MACS) that implements a dual level optimisation and a single level optimisation through a Pascoletti-Serafini scalarization. In DFET, the time domain is divided into a given number of segments, or elements, and the states and controls are approximated as arbitrary order polynomials on a spectral basis. DFET was successfully used to solve many difficult trajectory optimisation problems [3–5], and is a very robust transcription method with many interesting characteristics. As pointed out by Bottasso and Ragazzi [6], if used for forward time integration it is equivalent to some classes of implicit Runge-Kutta integration schemes. Moreover it can be extended to an arbitrary high order and supports full h-p adaptivity. MACS is a memetic evolutionary multi-objective optimisation algorithm in which a population of agents is initially seeded in the search space with a Latin Hypercube sampling. All agents can perform a set of individual actions to explore their neighborhood and improve their position. Non-dominated solutions are saved to an external archive. Some agents can, afterwards, perform social actions, exploiting the information coming from the archive or from other agents to collectively advance towards the Pareto front. Individual and social actions are repeated until a maximum number of function evaluations is reached. A special archiving strategy ensures a good distribution of points across the Pareto front.

The proposed approach is tested on a complex test case focusing on the optimal control of nominal ascent, re-entry and abort trajectory options for an airborne spaceplane launch system. Previous work looked at benchmarking ascent cases starting from the Goddard rocket problem [7].

It is interesting to note that although much research has been dedicated to the optimisation of rocket ascent trajectories (with the seminal work of Goddard [8] dating back almost a century), most of that effort has been dedicated to include more sophisticated physics [9–12] but little has been done on multi-objective optimal control. The only relevant work found was carried out by Pagano and Mooij [13] however the shape of the control law was defined a priori and only some of the parameters describing this shape were optimised. Moreover, only one cost function, the mass of the payload, was maximised while the other objectives were violations of the constraints.

With the renewed interest in the development of spaceplanes, from the far-term solution of a fully reusable single-stage-to-orbit spaceplane to the near-term options of partially-reusable vehicles where the first stage vehicle is flight-capable, the combination of aircraft and rocket flight profiles presents a challenging problem for the trajectory optimisation. Flight abort options also present an interesting combination of multiple objectives depending on where/when the failure occurs during the ascent [14]. Glide paths need to be designed that trade-off range for manoeuvrability while minimising heat and acceleration loading.

This paper will examine re-entry and abort scenarios for spaceplane-based launch systems using a multi-objective optimal control algorithm. In addition, a novel approach to the DFET transcription using Bezier curves is presented for the first time. This approach synergistically leverages several of the peculiar characteristics of Bezier curves and of the

DFET transcription, allowing for a convergent, smooth and non oscillating polynomial approximation of the controls even in case of bang-bang solutions.

II. Mathematical Models

The following section presents the mathematical models used to describe the vehicle dynamics and operative constraints.

A. Dynamical model

The vehicle dynamics are modelled as a 3DOF point mass moving in an Earth Centred reference frame [15, 16],

$$\dot{r} = v \sin\gamma \tag{1a}$$

$$\dot{\lambda} = \frac{v}{r\cos\theta}\cos\gamma\sin\psi \tag{1b}$$

$$\dot{\theta} = \frac{v}{r}\cos\gamma\cos\psi \tag{1c}$$

$$\dot{v} = \frac{F_T\cos\alpha - D}{m} - g\sin\gamma \tag{1d}$$

$$\dot{\gamma} = \frac{F_T\sin\alpha + L}{mv}\cos\beta + \left(\frac{v}{r} - \frac{g}{v}\right)\cos\gamma \tag{1e}$$

$$\dot{\psi} = \frac{F_T\sin\alpha + L}{mv\cos\gamma}\sin\beta + \frac{v}{r\cos\theta}\cos\gamma\sin\psi\sin\theta \tag{1f}$$

where r is the radial distance from the centre of the Earth to the vehicle, λ and θ are longitude and latitude, v is the magnitude of velocity in the ECI frame, γ and ψ are the flight path and azimuth angles, m is the mass of the vehicle, L and D are the aerodynamic lift and drag forces, and $g = \mu_E/r^2$ is the gravitational acceleration. The control variables are the angle of attack α and bank angle β of the vehicle.

The International Standard Atmosphere model was used to model the atmospheric temperature, pressure P_a, and density as a function of altitude $h = (r - r_E)$ assuming a spherical Earth model with a radius R_E, gravitational parameter μ_E and constant angular rotational velocity ω_E. The atmosphere was assumed to rotate with the same angular velocity as the Earth, so the aerodynamic quantities were computed using the velocity of the aircraft relative to the air with no wind (or other disturbances),

$$L = \frac{C_L\rho S_{ref} v_{rel}^2}{2} \tag{2}$$

$$D = \frac{C_D\rho S_{ref} v_{rel}^2}{2} \tag{3}$$

where $\mathbf{v}_{rel} = \mathbf{v} - \boldsymbol{\omega_E}\mathbf{r}$.

In order to limit the maximum static structural stresses, a limit on total acceleration is imposed,

$$\dot{v}^2 + v^2\left(\dot{\gamma}^2 + \dot{\theta}^2\right) \leq a_{max}^2 \tag{4}$$

The maximum magnitude of the acceleration vector, a_{max}, was set to $3g_0$.

B. Propulsion model

The thrust vector is assumed to be always aligned with the vehicle longitudinal body axis and is proportional to the vacuum thrust T_{vac} of the engine and modulated by a throttle control $\delta_T \in [0,\ 1]$. An additional term is added to account for the losses due to the difference between the nozzle's exit pressure P_e and the external atmospheric pressure P_a. The resulting model is,

$$F_T = \delta_T\left(T_{vac} - A_e\left(P_e - P_a\right)\right) \tag{5}$$

where A_e is the nozzle's exit area. For the test case here, a vacuum I_{sp} of 450 s is used with a vacuum thrust rating of 1350 kN and $A_e = 1.3937$ m^2. The mass flow rate of the propellent $\dot{m}_p$ is given by,

$$\dot{m}_p = \frac{\delta_T T_{vac}}{I_{sp} g_0} \tag{6}$$

As the on-board propellant mass is the only time-varying vehicle mass parameter, then the rate of change of the vehicle mass $\dot{m} = -\dot{m}_p$.

C. Aerodynamic model

Lift and drag coefficients were modelled as a non-linear least square best fit of digitized data curves of the X-34 vehicle [17] as functions of angle of attack α and Mach number M. The resulting models are of the form,

$$\begin{aligned} C_L(\alpha, M) &= P_{2,1}(\alpha) + P_{2,2}(\alpha)W_1(M) + P_{2,3}(\alpha)W_2(M) \\ C_D(\alpha, M) &= P_{3,3}(\alpha) + P_{3,4}(\alpha)W_3(M) + P_{3,3}(\alpha)W_3(M) \end{aligned} \tag{7}$$

where $P_{i,j}$ is the j^{th} polynomial of degree i of α with coefficients $(a_{j,0}, \cdots, a_{j,i+1})$ and W_i are Weibull distributions over Mach with parameters (λ_j, k_j) shifted by s_j, i.e.,

$$W_i = \frac{k_i}{\lambda_i}\left(\frac{M - s_i}{\lambda_i}\right)^{k_i - 1} e^{-\left(\frac{M - s_i}{\lambda_i}\right)^{k_i}} \tag{8}$$

Weibull distributions have a single peak and a zero derivative for high Mach numbers, thus were chosen for their similarity with respect to the profile of C_L and C_D data over Mach and because they naturally decay to 0 with zero slope for large values of the argument. Thus, they allow to safely evaluate these aerodynamic models even for Mach numbers above the tabulated data and will consistently give no dependence over Mach for those ranges.

Coefficients for this aerodynamic model are given in Table 1 in the Appendix. Figure 1 shows the overall agreement between the model and the data points. The R^2 value of the non-linear fit is over 0.99 for both models. As no data was provided in the rectangular area below $\alpha \leq 20^\circ$ and over $M \geq 3$, the smooth constraint

$$\left(\frac{\alpha - 35}{15}\right)^8 + \left(\frac{M - 30}{27}\right)^8 - 1 \leq 0 \tag{9}$$

was imposed to exclude that area. Another path constraint was imposed on all trajectories to ensure $M \geq 0.3$ to exclude this area where no data was available and the models extrapolated poorly.

As the vehicle is not expected to fly in either of these regions, these constraints should not influence the resulting trajectories.

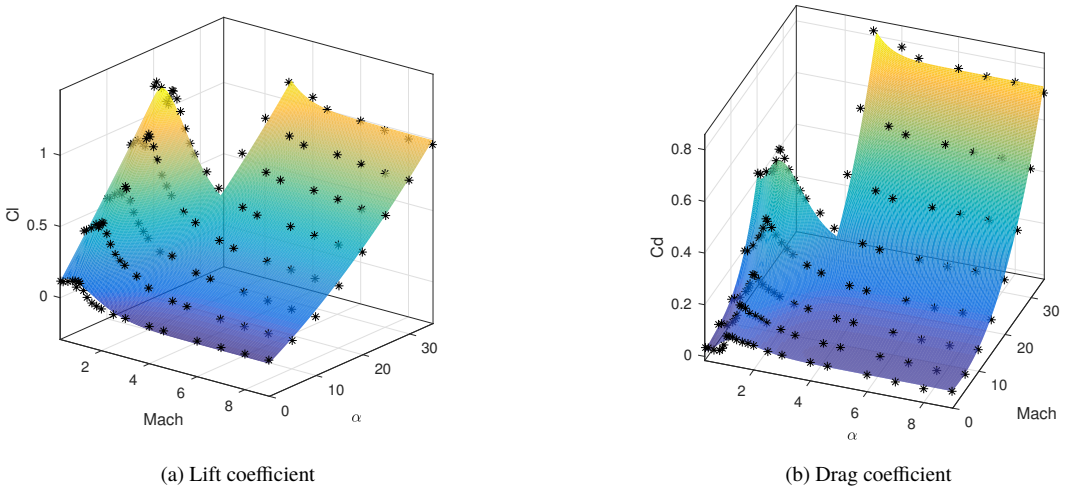

(a) Lift coefficient

(b) Drag coefficient

Fig. 1 Aerodynamic coefficients: data points as black dots and non-linear fit surfaces for C_L and C_D.

D. Thermal model

In Betts [15], a semi-empirical correlation for the heat flux at the nose,

$$Q = \left(c_0 + c_1\alpha + c_2\alpha^2 + c_3\alpha^3\right) c_4 \sqrt{\rho}\,(c_5 v)^{c_6} \leq Q_{max} \tag{10}$$

was employed for the Space Shuttle re-entry trajectory optimisation problem, where Q_{max} is the maximum allowed value, with the coefficients reported in the reference. Although very simple, the model was deemed adequate for the re-entry case analysed in the literature and was used also in the present study. Moreover, a multi-objective extension of the problem presented in Betts [15] is solved in Section V as validation case of the current algorithm. For the ascent and abort trajectory optimisation of the new vehicle, the same limit on the heat flux of 800 kW/m^2 is imposed.

E. Wing mass model and wing loading constraints

Wing surface area was considered an optimisation variable. To account for the change in mass, the mass estimation relationship from Rohrschneider [18] was used.

$$m_{wing} = \left(N_z m_{land} \frac{1}{1 + \eta \frac{S_{body}}{S_{exp}}}\right)^{0.386} \left(\frac{S_{exp}}{t_{root}}\right)^{0.572} \left(K_{wing} b_{str}^{0.572} + K_{ct} b_{body}^{0.572}\right) \tag{11}$$

where N_z is the ultimate load factor (1.5 times the maximum allowed wing loading), m_{land} is the landed mass, S_{body} is the surface of the fuselage, S_{exp} is the surface of the exposed part of the wing, t_{root} is the wing thickness at the root, b_{str} is the structural wing span at half chord line, b_{body} is the fuselage width and η, K_{wing}, K_{ct} are constants depending on the constructive solution and materials of the wing. The constants were assumed to have the smallest values proposed in the list, while the geometrical parameters were computed by estimating the geometry of the X-34 vehicle and scaling them with respect to the reference wing area of the test case to maintain geometric similarity. The landed mass m_{land} was assumed to be equal to the unknown initial mass of the vehicle $m(t_0)$, while the final mass was set equal to $m(t_f) = m_{wing} + m_{str}$, where m_{str} is the structural mass of the vehicle plus the payload, without the wings, and has a fixed value of 10 tonnes.

Since an optimisation of the gross take-off mass could result in a reduction of wing area, the constraint

$$\frac{m_0}{S} \leq W_{L,max} \tag{12}$$

was imposed to limit the maximum allowed wing loading $W_{L,max}$ to 700 kg/m^2.

F. Dynamic pressure limits

A limit on the dynamic pressure encountered by the vehicle is imposed as

$$\frac{1}{2}\rho v_{rel}^2 \leq q_{max} \tag{13}$$

where q_{max} is the maximum allowed value and is set to 60 kPa.

III. Direct Transcription of Multi-Objective Optimal Control Problems

Multi-objective optimal control problems can be formulated as:

$$\begin{aligned}
&\min_{\mathbf{u}\in U} \mathbf{J} = [J_1, J_2, ..., J_i ..., J_m]^T \\
&s.t. \\
&\dot{\mathbf{x}} = \mathbf{F}(\mathbf{x}, \mathbf{u}, t) \\
&\mathbf{g}(\mathbf{x}, \mathbf{u}, t) \geq 0 \\
&\boldsymbol{\psi}(\mathbf{x}_0, \mathbf{x}_f, t_0, t_f) \geq 0 \\
&t \in [t_0, t_f]
\end{aligned} \tag{14}$$

where $\mathbf{J}$ is a vector of objectives J_i that are functions of the state vector $\mathbf{x} : [t_0, t_f] \rightarrow \mathbb{R}^n$, control variable $\mathbf{u} \in L^\infty$ and time t. The functions $\mathbf{x}$ belong to the Sobolev space $W^{1,\infty}$ while the objective functions are $J_i : \mathbb{R}^{n+2} \times \mathbb{R}^p \times [t_0, t_f] \longrightarrow \mathbb{R}$.

The objective vector is subject to a set of dynamic constraints with $\mathbf{F} : \mathbb{R}^n \times \mathbb{R}^p \times [t_0, t_f] \longrightarrow \mathbb{R}^n$, algebraic constraints $\mathbf{g} : \mathbb{R}^n \times \mathbb{R}^p \times [t_0, t_f] \longrightarrow \mathbb{R}^s$, and boundary conditions $\boldsymbol{\psi} : \mathbb{R}^{2n+2} \longrightarrow \mathbb{R}^q$. Note that the problem in Eq. (14) generally is non-smooth and can include a number of additional static parameters.

A. Problem Transcription

Problem (14) is transcribed into a multi-objective, non-linear programming problem via DFET [1]. DFET was initially proposed by Vasile [3] in 2000 and uses finite elements in time on spectral bases to transcribe the differential equations into a set of algebraic equations. Finite Elements in Time (FET) for the indirect solution of optimal control problems were initially proposed by Hodges and Bless [19], and during the late 1990s evolved to the discontinuous version. As pointed out by Bottasso and Ragazzi [6], FET for the forward integration of ordinary differential equations are equivalent to some classes of implicit Runge-Kutta integration schemes, can be extended to arbitrary high-order, are very robust and allow full h-p adaptivity. In the past decade, direct transcription with FET on spectral bases has been successfully used to solve a range of difficult problems: from the design of low-thrust multi-gravity assist trajectories to Mercury [4] and to the Sun [5], to the design of weak stability boundary transfers to the Moon, low-thrust transfers in the restricted three body problem and optimal landing trajectories to the Moon [3].

For each individual cost function consider the following Bolza's problem:

$$\min_{\mathbf{u} \in U} J_i = \alpha_i \phi_i(\mathbf{x_0}, \mathbf{x_f}, t_0, t_f) + \beta_i \int_{t_0}^{t_f} L_i(\mathbf{x}, \mathbf{u}, t) dt \tag{15}$$

where α_i and β_i are positive weights. In multi-objective optimisation this formulation corresponds to a weighted sum scalarisation, which is known to be unable to represent points on non-convex regions of the Pareto front. To avoid this problem, this paper only considers cases with ($\alpha_i = 1$, $\beta_i = 0$) or ($\alpha_i = 0$, $\beta_i = 1$). The differential constraints can be recast in weak form and integrated by parts leading to,

$$\int_{t_0}^{t_f} \mathbf{w}^T \mathbf{x} + \mathbf{w}^T \mathbf{F}(\mathbf{x}, \mathbf{u}, t) dt - \mathbf{w}_f^T \mathbf{x}_f^b + \mathbf{w}_0^T \mathbf{x}_0^b = 0 \tag{16}$$

where $\mathbf{w}$ are the generalised weight functions and $\mathbf{x}^b$ are the boundary values of the states, that may be either imposed or free. Let the time domain D be decomposed into N finite elements such that

$$D = \bigcup_{j=1}^{N} D_j(t_{j-1}, t_j) \tag{17}$$

and parametrise, over each D_j, the states, controls and weight functions as

$$\mathbf{x}(t) = \mathop{\cup}_{j=1}^{N} \mathbf{X}_j = \mathop{\cup}_{j=1}^{N} \sum_{s=0}^{l} f_{sj}(t)\, \mathbf{x}_{sj} \tag{18a}$$

$$\mathbf{u}(t) = \mathop{\cup}_{j=1}^{N} \mathbf{U}_j = \mathop{\cup}_{j=1}^{N} \sum_{s=0}^{m} g_{sj}(t)\, \mathbf{u}_{sj} \tag{18b}$$

$$\mathbf{w}(t) = \mathop{\cup}_{j=1}^{N} \mathbf{W}_j = \mathop{\cup}_{j=1}^{N} \sum_{s=0}^{l+1} h_{sj}(t)\, \mathbf{w}_{sj} \tag{18c}$$

where $\mathop{\cup}_{j=1}^{N}$ denotes the juxtaposition of the polynomials defined over each sub-interval, and the functions f_{sj}, g_{sj} and h_{sj} are chosen among the space of polynomials of degree l, m and $(l+1)$ respectively. It is practical to define each D_j over the normalised interval $[-1, 1]$ through the transformation,

$$\tau = 2 \frac{t - \frac{t_j - t_{j-1}}{2}}{t_j - t_{j-1}} \tag{19}$$

This way the domain of the basis function is constant and irrespective of the size of the element and also overlaps with the interval of the Gauss nodes that will be employed for the integration of the dynamics. Substituting the definitions of the polynomials into the objective functions and integrating with Gauss quadrature formulas leads to,

$$\tilde{J}_i = \alpha_i \phi_i(\mathbf{X}_0^b, \mathbf{X}_f^b, t_0, t_f) + \beta_i \sum_{j=1}^{N} \sum_{k=1}^{l+1} \sigma_k L_i(\mathbf{X}_j(\tau_k), \mathbf{U}_j(\tau_k), \tau_k) \frac{\Delta t}{2} \tag{20}$$

and for the variational constraints leads for every element to the system

$$\sum_{k=1}^{l+1} \sigma_k \left[\mathbf{W}_j(\tau_k)^T \mathbf{X}_j(\tau_k) + \mathbf{W}_j(\tau_k)^T \mathbf{F}_j(\tau_k) \frac{\Delta t}{2} \right] - \mathbf{W}_{p+1}^T \mathbf{X}_j^b + \mathbf{W}_1^T \mathbf{X}_j^b = 0 \tag{21}$$

where τ_k and σ_k are the Gauss nodes and weights, and $\mathbf{F}_j(\tau_k)$ is the shorthand notation for $\mathbf{F}\left(\mathbf{X}_j(\tau_k), \mathbf{U}_j(\tau_k), \tau_k\right)$. Algebraic, path constraints and boundary conditions are evaluated at the Gauss nodes, as for the objective functions. Thus, the optimal control problem in Eq. (15) was transcribed into the non-linear programming (NLP) problem (20), which in compact form reads as:

$$\begin{aligned} &\min_{\mathbf{p} \in \Pi} \tilde{\mathbf{J}}(\mathbf{x}_s, \mathbf{p}) \\ &s.t. \\ &\mathbf{c}(\mathbf{x}_s, \mathbf{p}) \geq 0 \end{aligned} \tag{22}$$

where the vector $\mathbf{x}_s$ contains all the values for the states evaluated at the integration nodes τ_k, $\mathbf{p} = [\mathbf{u}_s, \mathbf{x}_0, \mathbf{x}_f, t_0, t_f]^T$ collects all the static and dynamic control variables.It is worth noting that the DFET transcription is very flexible and allows to choose any basis for the states, controls and test functions, and the basis could also be different for every variable. Similarly it is possible to employ several choices for the type of quadrature nodes.

B. Choice of quadrature rule

Bottasso and Ragazzi [6] gave a variational interpretation of some implicit Runge-Kutta schemes, and noticed that depending on the choice of the nodes for the Gauss quadrature, different equivalent Runge-Kutta schemes could be generated by FET. The choice of the quadrature nodes affects its stability and order of convergence properties: Gauss-Legendre quadrature has the highest order of convergence for a given number of quadrature points and is algebraically stable and symplectic for Hamiltonian systems, Gauss-Lobatto quadrature is A-stable, while Gauss Radau Left is L-stable and algebraically stable. The choice of the quadrature rule should thus consider the properties of the system at hand: in this case no stiff nature is apparent so Gauss-Legendre quadrature was chosen for its highest order of accuracy and the algebraic stability property.

C. Choice of basis functions

In the DFET literature, the basis is typically generated through a Lagrange interpolation on the quadrature nodes (either Gauss-Legendre or Gauss-Lobatto):

$$f_{sj}(\tau) = \prod_{k=0, k \neq s}^{l} \frac{\tau - \tau_k}{\tau_s - \tau_k} \tag{23}$$

Since the basis has to be evaluated only at the quadrature nodes, this choice ensures that $f_{sj}(\tau_k) \neq 0$ only if $s = k$. This should generally result in a good sparsity pattern for the Jacobian of the constraints. However a proper implementation of DFET already ensures a highly sparse block diagonal Jacobian of the constraints regardless of the choice of the basis. Thus the further improvement due to this particular choice is expected to be modest, especially as the problem size increases, because it can only act on the individual block. In other words, this basis seems to provide marginal benefits overall. Other polynomial bases could instead provide different and maybe more significant benefits, but to the authors' knowledge the most commonly used polynomial bases are Lagrange interpolation on either the Legendre or the Lobatto nodes.

In the following we propose the use of a different basis and compare it with the typical ones. In [1, 20, 21] the typical Lagrange interpolation basis was used. When solving the minimum time trajectory injection problem, which has

a bang-bang solution, a high order polynomial representation of the controls resulted in highly oscillating results across the discontinuity, exceeding the upper or lower bound even if the computed nodal solution was correct. The possibility of generating these out of bounds oscillatory solutions is not restricted to bang-bang solutions but, as will be shown, also happens when a control variable reaches a maximum or minimum value for a finite amount of time and then gradually takes different values within the same time element. One way to address the problem, as shown by Vasile [1], is by using an h-p adaptive strategy. This approach, which is iterative and changes the size of the NLP, poses a series of difficulties to the current implementation of MACS. Another solution, which can work with MACS, is to use a high number of elements and restricting the control polynomials to be order 1. This approach however negates one of the most appealing characteristics of DFET transcription, i.e., the use of a relatively small number of high order polynomials.

We here propose for the first time in the DFET literature (to the authors' knowledge), the use of Bernstein polynomials as a basis, and will show that it can by construction solve the reported issues. A Bernstein basis of order n is defined as

$$B_{\nu,n}(t) = \binom{n}{\nu} t^{\nu}(1-t)^{n-\nu} \qquad 0 \leq \nu \leq n, 0 \leq t \leq 1 \tag{24}$$

Since the resulting curves will be integrated through Gauss quadrature, whose nodes are defined on $[-1,\ 1]$, Bernstein polynomials must also be redefined on the interval $[-1,\ 1]$.

$$\tilde{B}_{\nu,n}(\tau) = B_{\nu,n}(t) \qquad \tau = 2t - 1 \tag{25}$$

Substituting (25) into (18) we obtain

$$\mathbf{x}(\tau) = \bigcup_{j=1}^{N} \mathbf{X}_j = \bigcup_{j=1}^{N} \sum_{s=0}^{l} \tilde{B}_{sj}(\tau)\, \mathbf{x}_{sj} = \bigcup_{j=1}^{N} \mathcal{B}_j(\tau) \tag{26a}$$

$$\mathbf{u}(\tau) = \bigcup_{j=1}^{N} \mathbf{U}_j = \bigcup_{j=1}^{N} \sum_{s=0}^{m} \tilde{B}_{sj}(\tau)\, \mathbf{u}_{sj} = \bigcup_{j=1}^{N} \mathcal{C}_j(\tau) \tag{26b}$$

$$\mathbf{w}(\tau) = \bigcup_{j=1}^{N} \mathbf{W}_j = \bigcup_{j=1}^{N} \sum_{s=0}^{l+1} \tilde{B}_{sj}(\tau)\, \mathbf{w}_{sj} = \bigcup_{j=1}^{N} \mathcal{D}_j(\tau) \tag{26c}$$

Thus, if the basis is composed by Bernstein polynomials the resulting state curves $\mathcal{B}_j(\tau)$, control curves $\mathcal{C}_j(\tau)$ and test curves $\mathcal{D}_j(\tau)$ are by definition Bezier curves and as such, they have the convex hull and variation diminishing property. The convex hull property guarantees that the resulting curve is enclosed in the convex hull of the polygonal chain generated by the weights at the control nodes τ_k. This ensures that the solution curves will be completely within the allowed bounds, not only at the quadrature nodes. The variation diminishing property guarantees instead that the resulting curve will oscillate no more than the control polygon. Thus, if the polygonal chain connecting the nodal values of the controls of a bang-bang solution switches only once in an element, the resulting curve will be monotonic.

The effect of these properties, along with the quantification of the impact of the choice of this basis on the overall sparsity of the Jacobian of the constraints, will be analysed in Section V.

It is worth noticing that the use of Bezier curves to solve optimal control problems has already been proposed in [22–26] and several others. Here, however, Bezier curves are a natural result of the choice of Bernstein polynomials for the basis, which were chosen precisely because the resulting Bezier curves have the convex hull and variation diminishing property. It is the authors' opinion that this fact has apparently received very little attention in the literature.

IV. Solution Approach

Problem (22) is solved with MACS [2, 27] a memetic multi-objective optimisation algorithm that combines a stochastic agent-based search with a local (gradient in this case) refinement of the solutions [7, 20, 21]. The agent-step solves the following two-level problem:

$$\begin{aligned} &\min_{\mathbf{p}^*} \tilde{\mathbf{J}}(\mathbf{x}^*, \mathbf{p}^*) \\ &s.t. \\ &(\mathbf{x}^*, \mathbf{p}^*) = \operatorname{argmin} \{ f(\mathbf{x}_s, \mathbf{p}) \,|\, \mathbf{c}(\mathbf{x}_s, \mathbf{p}) \geq 0 \} \end{aligned} \tag{27}$$

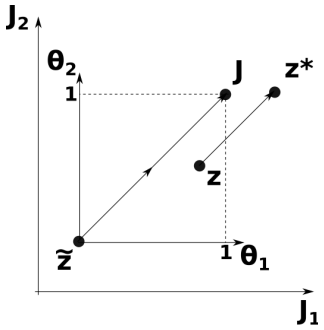

Fig. 2 Schematic representation of descent directions λ_i and target point $\tilde{\mathbf{z}}$ for agent j

Problem (27) defines two different optimisation problems at two different levels. The outer level handles the objective vector $\tilde{\mathbf{J}}$ and the control parameter $\mathbf{p}^*$, generating tentative solutions using some evolutionary heuristics. This tentative solution is fed into the inner level problem, whose goal is to find the state and control vectors $\mathbf{x}^*$ and $\mathbf{p}^*$ that satisfy the constraints $\mathbf{c}$ and minimise an inner cost function f. The inner cost function is the displacement from the initial $\mathbf{p}$ provided by the outer level. Thus, the inner level will look for the feasible solution closest to the tentative solution generated by the upper level. The upper level then receives a solution $(\mathbf{x}^*, \mathbf{p}^*)$, that satisfies the constraints, and proceeds by evaluating the objective functions associated to the feasible solutions.

As part of its selection criteria, MACS translates the outer multi-objective problem into scalar form by using Chebyshev scalarisation:

$$\begin{aligned} &\min_{\mathbf{p}^*} \max_i \ \lambda_{ij}[\tilde{J}_{ij} - z_i] \\ &s.t. \\ &(\mathbf{x}^*, \mathbf{p}^*) = \text{argmin}\,\{f(\mathbf{x}_s, \mathbf{p}) | \mathbf{c}(\mathbf{x}_s, \mathbf{p}) \geq 0\} \end{aligned} \tag{28}$$

Since this problem is not smooth, it's not suitable for a gradient based refinement. Thus, instead of the Chebychev scalarisation, the following equivalent problem for each agent j is solved:

$$\begin{aligned} &\min_{\alpha>0} \ \alpha \\ &s.t. \\ &\lambda_{ij}\vartheta_{ij}(\overline{\mathbf{x}}, \overline{\mathbf{p}}) \leq \alpha \qquad i = 1, .., m \\ &\mathbf{c}(\overline{\mathbf{x}}, \overline{\mathbf{p}}) \geq 0 \end{aligned} \tag{29}$$

where λ_j is the vector of Chebyshev weights associated to agent j^{th}, ϑ_{ij} is the i^{th} component of the rescaled objective vector of the j^{th} agent and α is a slack variable. This reformulation of the problem is constraining the agent's move, in criteria space, within the descent cone defined by the point $\alpha\mathbf{d}_j + \zeta_j$ along the direction $\mathbf{d}_j = (1/\lambda_{1j}, ..., 1/\lambda_{ij}, ..., 1/\lambda_{mj})$. The rescaled objective vector is defined as:

$$\vartheta_{ij}(\overline{\mathbf{x}}, \overline{\mathbf{p}}) = \frac{\tilde{J}_{ij}(\overline{\mathbf{x}}, \overline{\mathbf{p}}) - \tilde{z}_i}{z^*_{ij} - \tilde{z}_i} \qquad i = 1, .., m \tag{30}$$

where $\mathbf{z}^*_j$ is equal to $\tilde{\mathbf{J}}_j(\overline{\mathbf{x}}, \overline{\mathbf{p}}^c)$ and $(\overline{\mathbf{x}}, \overline{\mathbf{p}}^c)$ is the initial guess for the solution of (29). This way the components of $\vartheta_j(\overline{\mathbf{x}}, \overline{\mathbf{p}})$ have value 1 at the beginning of the local search and if the agent converges to the utopia point $\tilde{\mathbf{z}}$, the components of $\vartheta_j(\overline{\mathbf{x}}, \overline{\mathbf{p}})$ become all equal to 0. The target points $\tilde{\mathbf{z}}_j$ and descent directions $\mathbf{d}_j$ are generated as follows: with reference to Figure 2, the vector $\mathbf{z}^* - \mathbf{z}$ from the utopia point to the nadir point is computed. Then, for each agent, a point $\tilde{\mathbf{z}}$ is computed by translating its initial position $\mathbf{J}$ by $-2(\mathbf{z}^* - \mathbf{z})$. The distance from the point $\mathbf{J}$ to $\tilde{\mathbf{z}}$ is thus twice large as the diagonal of the bounding box defined from the utopia and nadir point. Directions $\boldsymbol{\lambda}_j$ are computed for all agents following a scalarised problem involving more than one objective as $\mathbf{d} = (\sqrt{2}, \sqrt{2})^T$, while for agents solving either of the two orthogonal problems are simply kept as $\mathbf{d} = (1, 0)^T$ or $\mathbf{d} = (0, 1)^T$. However, the agents following the orthogonal subproblems can also swap direction if they cannot further improve along the current direction. In that case, a constraint is imposed so that the feasible region strongly dominates the current solution.

From the normalisation one can derive the components of the vector ζ_j:

$$\zeta_{ij} = \frac{z_i}{z^*_{ij} - \tilde{z}_i} \qquad i = 1, .., m \tag{31}$$

Problem (28) and (29) are equivalent and lead to the same optimal solution. In fact the following theorem holds true [28]:

Theorem IV.1 *A point* $(\alpha, \mathbf{p}) \in \mathbb{R} \times \Pi$ *is a minimal solution of* (29) *with* $\mathbf{z} \in \mathbb{R}^m$, $z_j < \min_{\mathbf{p}\in\Pi} J_j(\mathbf{p}), j = 1, ..., m$, *and* $\lambda \in int(\mathbb{R}^m_+)$ *if and only if* $\mathbf{p}$ *is a solution of* (28).

Therefore, by combining (28) in the search phase with (29) in the refinement phase, the algorithm has a smooth transition from the agent-step, that provides global convergence and coverage of the Pareto set, to the constrained local search that guarantees local optimality.

V. Test cases

Atmospheric re-entry trajectories of space vehicles are a typical example of optimal control problems with significant practical importance, due to the inherent deep non-linearity of the dynamics and the necessity to satisfy several path constraints due to safety considerations. Before analysing two different test cases involving all the complexities of deeply non-linear systems, the effects of choosing Bernstein bases over Lagrange interpolating bases for a much simpler system will be presented. This will provide a justification for their use for the more complex test cases, for which the benefits provided by this different set of basis function will be evident. The code and all the test cases in this paper were implemented in Matlab 2017b and run on a laptop with an Intel i7 7770HQ CPU under Windows 10.

A. Comparison of Legendre basis with Bernstein basis

In [1, 20, 21] the ascent problem was proposed as a simple test case to validate the DFET transcription method. The dynamics in (32) below are a simplification of the problem described by (1) because it deals with the ascent of a point mass in a plane subject only to a constant gravitational acceleration in an inertial frame, and controlled by the changing the angle u of a constant thrust vector.

$$\dot{x} = v_x \tag{32a}$$
$$\dot{v}_x = a\cos(u) \tag{32b}$$
$$\dot{y} = v_y \tag{32c}$$
$$\dot{v}_y = -g + a\sin(u) \tag{32d}$$

Figure 3 shows the control profiles for the minimum time optimal control of an ascent problem described by Vasile in [1, 21], discretised with four elements of order 6 for both states and controls, and using either Lagrange interpolation on Legendre nodes or Bernstein bases for both states and controls. For the Lagrange-Legendre case, the nodal solutions, marked with stars in the figures, assume only values within $[-\frac{\pi}{2}, \frac{\pi}{2}]$ but the polynomial approximation of the controls outside of the collocation nodes goes out of bounds. This is normal since collocation methods only compute the solution at the collocation nodes. The solution computed using Bernstein polynomials instead shows no oscillation nor bounds violations on the whole domain. For order 6 of both bases, Figure 4 shows the sparsity pattern of the Jacobian of the constraints. It is apparent from the figures that the overall structure of the Jacobian is the same, with sparse blocks for the dynamics, thin columns indicating weak matching constraints between elements, and a final full row for the free final time. The figures also report the number of non-zero elements: Legendre basis of order 6 has a sparsity of 11.32%, while Bernstein basis of the same order has a sparsity of 11.51%, a very marginal increase. Similarly, if one increased the order to 12, Legendre basis would display a sparsity of 9.79% while the sparsity for Bernstein basis would be 11.31%. Indeed as the order reduces the sparsity of the two methods tends to align, vice versa the difference becomes more pronounced as the order increases.

B. Optimal Descent Trajectory

The first test case is based on a benchmark problem from literature by Betts [15] who analysed the unpowered re-entry of a Space Shuttle-like vehicle controlled by changing the angle of attack α and bank angle β. The dynamical

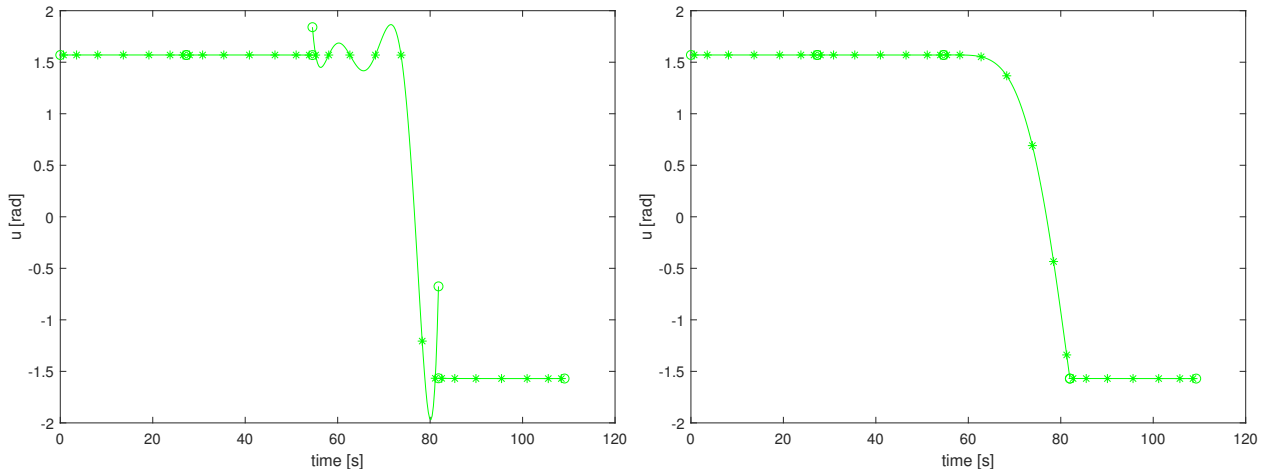

(a) Legendre order 6

(b) Bernstein order 6

Fig. 3 Time-history of the controls for the minimum time solution of ascent problem [3, 21] discretised with 4 DFET elements with the same order for states and controls. Nodal solutions marked with *, solid line for the evaluated polynomial representation.

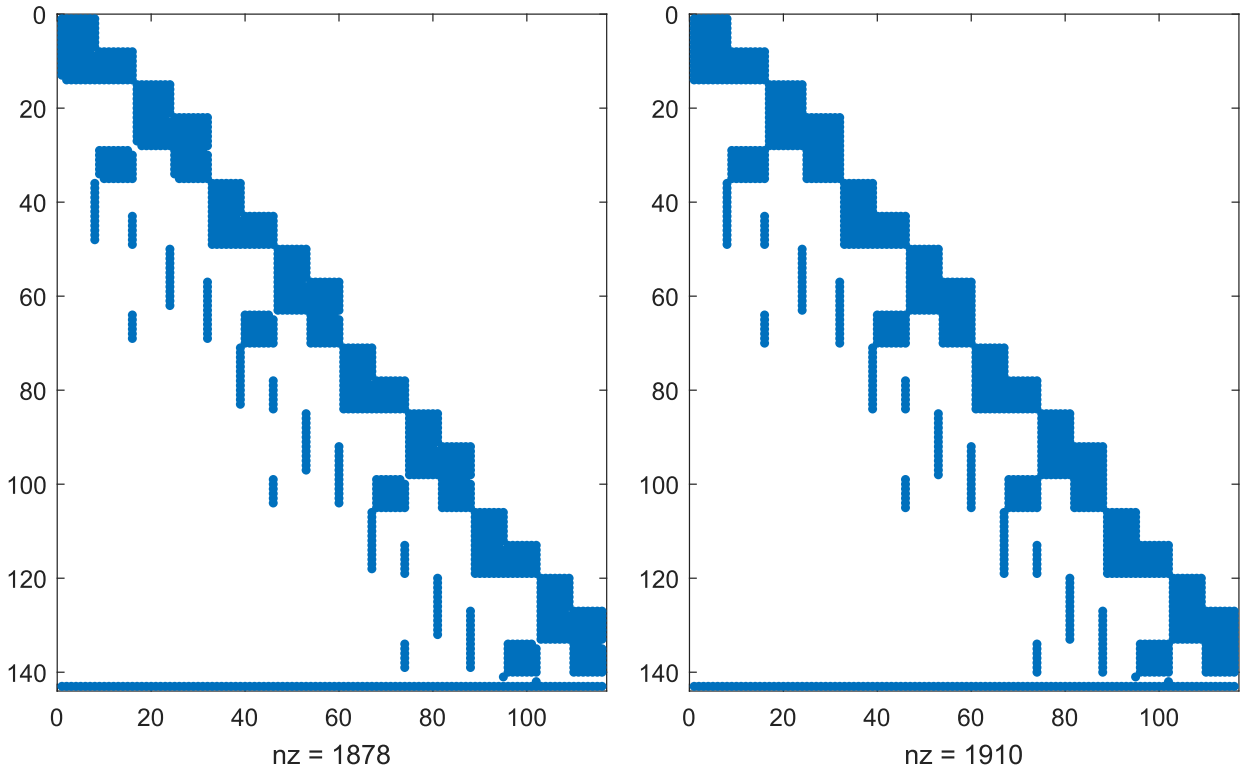

(a) Legendre order 6 for states and controls

(b) Bernstein order 6 for states and controls

Fig. 4 Sparsity pattern of the Jacobian of the constraints for the minimum time solution of ascent problem [3, 21] discretised with 4 DFET elements with the same order for states and controls.

model is equivalent to (1), with $F_T = 0$ and no mass variation due to propellant consumption. As in the reference, a linear/parabolic aerodynamic model and exponential atmospheric model were used, and the constraints on the accelerations were simplified to box constraints on the flight path and heading angle rates: $-0.2 \leq \dot{\gamma} \leq 0.2$ deg/s and $-0.2 \leq \dot{\chi} \leq 0.2$ deg/s. For consistency with respect to the reference, dynamic pressure was left unconstrained.

Starting from a given position, attitude and velocity, the problem was formulated with constraints to reach a final altitude, velocity and flight path angle while staying below a threshold level for the heat flux. Two different objectives were optimised in the reference: the maximum cross-range and the minimum peak heat flux. These two problems are reformulated here as a single multi-objective test case to show the trade-off between the two objectives and the resulting families of trajectories and control laws:

$$\min_{t_f,u} [J_1,\ J_2]^T = \left[-\theta_f,\ \max q\right]^T \tag{33}$$

Following the reference, the non-smooth problem $\min \max(q)$ was reformulated as a soft constraint minimisation of a slack variable q_u, resulting in the smooth problem

$$\begin{aligned} &\min_{t_f,u} [J_1,\ J_2]^T = \left[-\theta_f,\ q_u\right]^T \\ &s.t \\ &q \leq q_u \end{aligned} \tag{34}$$

The problem was discretised using 6 Gauss-Lobatto finite elements of order 9 for both states and controls, resulting in 121 optimisation parameters for the outer level (120 for to the control variables, and 1 for the free final time), and 484 total variables for the single level and inner level NLP. A limit of 20000 function evaluations was given to the optimiser, with gradient based single level refinement taking place every 10 iterations and at the final iteration.

Figure 5 shows the Pareto front with 10 nominal solutions, while Figures 6–9 show altitude, velocity, L/D ratio, heat flux, angle of attack, bank angle and the rates of change for the flight path and azimuth angles for each of the 10 Pareto optimal solutions.

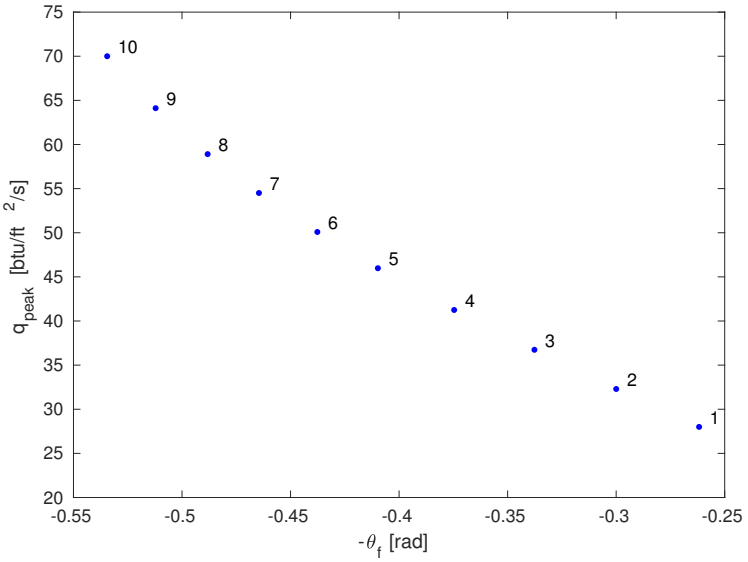

Fig. 5 Pareto front showing both objective functions of minimum heat flux q_{peak} and maximum downrange θ_f

The method is able to find both single objective solutions found in the reference without any externally supplied guess, and is able to give an evenly spread Pareto front. More function evaluations would result in an even better spreading. Solution 3 and 5 present some small imperfections due to the NLP solver reaching the minimum step size before optimality, but these imperfections do not diminish the validity of the proposed algorithm and could be bypassed by either using another solver or by simply using more function evaluations to allow the NLP solver to start from different nearby solutions.

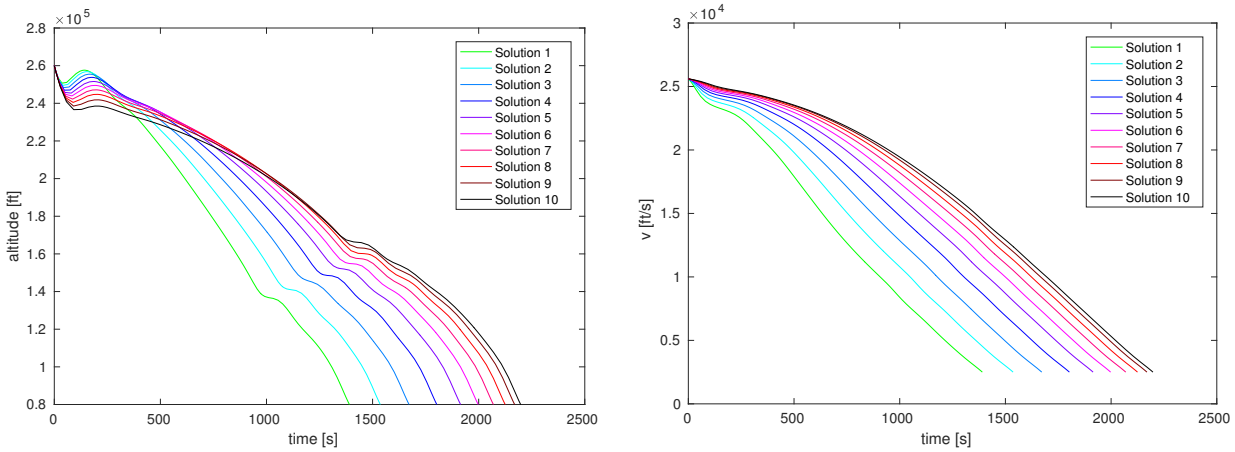

(a) Altitude (b) Velocity

Fig. 6 Time-history of the altitude and velocities for each of the 10 solutions shown on the Pareto front

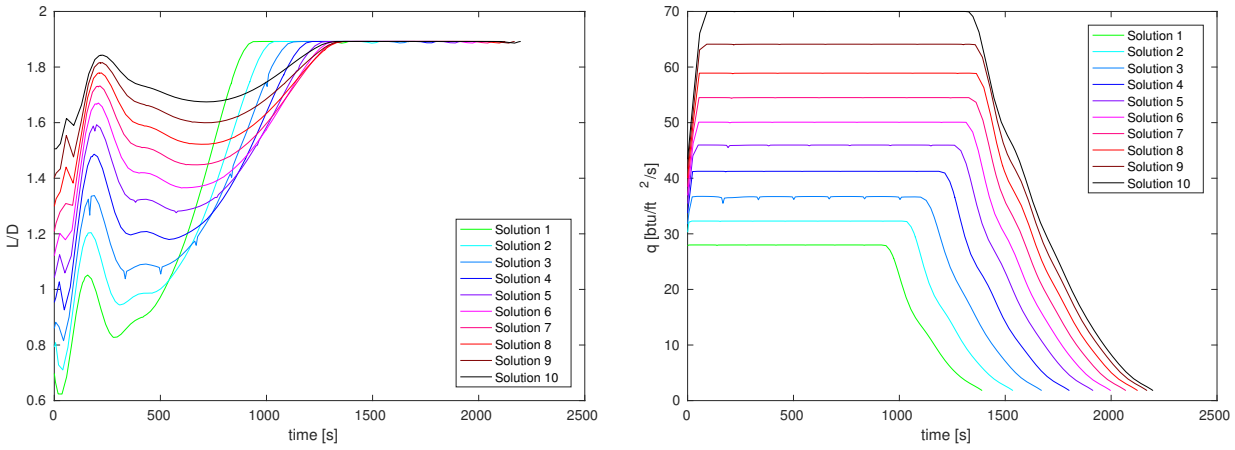

(a) Lift-to-drag (b) Heat flux

Fig. 7 Time-history of the lift to drag ratio heat flux for each of the 10 solutions shown on the Pareto front

A clear trend emerges from the solutions of the multi-objective problem: the minimum peak heat flux solution is also the shortest in time, and longer re-entries impose higher peak heat fluxes. This is due to the initial skip in the trajectory, which is more pronounced for the shorter time re-entries and causes the velocity to decrease faster but at the price of having then less energy and time to maximise the downrange. The peak heat flux is bounded from below by its initial value, so no further reductions are possible without changing the initial conditions. In terms of controls, it is interesting to notice that all trajectories share a similar profile: an initial peak heat flux containment phase, with high bank and high angle of attack, followed by a maximum aerodynamic efficiency phase to maximise the downrange when heat flux is no longer a concern. Angular rates are well below the threshold value along all the trajectories.

C. Optimal Ascent and Abort Scenarios

For the second test case, we follow a robust multidisciplinary design approach for a hypothetical reusable spaceplane. To simplify the analysis, the vehicle is assumed to be air-dropped by a carrier aircraft at an altitude of 10 km and a velocity of 200 m/s flying eastbound along the equator, and will target a circular equatorial parking orbit with 100 km altitude. One optimisation criterion is the minimisation of the spaceplane initial mass, and will involve finding not only the optimal trajectory and control law, but also the optimal sizing of the wing area and initial flight path angle, which

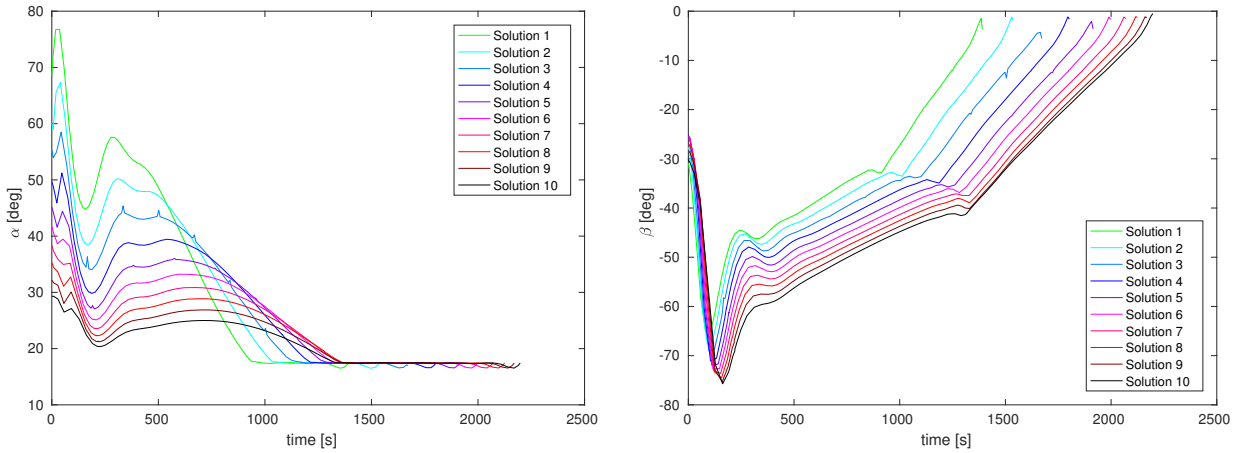

(a) Angle of attack

(b) Bank angle

Fig. 8 Time-history of the controls for each of the 10 solutions shown on the Pareto front

was left free as an optimisation variable and bounded between −10 and 10 degrees.

As one of the advantages of a winged launcher with respect to a conventional vertically-launched rocket is better manoeuvrability, it is interesting to study how it performs in an emergency case, and what design and trajectory options would provide better abort options. Here we assume that an engine failure will occur at a specific time t_{fail}, after which the engine will not be able to provide any thrust. To study the worst case, no fuel dumping was allowed.

Instead of performing a separate ascent and abort trajectory optimisation as in Toso and Maddock [14], a coupled, multi-phase multi-objective approach was followed. The mission was divided into three phases: the first phase from t_0 to t_{fail} considers the normal ascent trajectory before the failure occurs. At t_{fail}, two parallel branches are considered each taking into account one possibility: one option is phase 2 where the engine is still working and the spaceplane will ascend to its target orbit as efficiently as possible, while the second option is phase 3 where the engine has failed and the spaceplane will perform an emergency landing. As the vehicle is flying along the equator, the downrange can be measured in terms of the angular difference in latitude. The problem can thus be formulated as,

$$\min_{t_f,u}[J_1,\ J_2]^T = \left[m_{0,1},\ -(\lambda_{f,3} - \lambda_{0,3})\right]^T \tag{35}$$

where $m_{0,1}$ indicates the mass of the vehicle at the beginning of phase 1, while $\lambda_{0,3}$ and $\lambda_{f,3}$ indicate the latitude of the vehicle at the beginning and at the end of phase 3.

This coupled multi-objective multi-phase formulation allows a robust optimisation of the ascent trajectory because the abort scenario is automatically included in the sizing process and the trade-off drivers between the nominal performance and the abort manoeuvre safety are explicitly sought for. Alternate ways would be to consider more than one branching point or to consider a single unknown worst case branching point. Both these approaches require significantly larger computational cost. The first would require a many-objective optimisation approach (one maximisation of downrange per each abort branch) and the second would require solving an extremely complex multi-objective max(min(max)) optimal control problem, to maximise the worst case maximum downrange and minimise the initial mass. As it is expected that the worst case failure is in the first stage of the ascent trajectory when the vehicle has a low altitude and velocity and thus limited time and energy, the approach here followed seems a good compromise between computational cost and reliability of the results.

In the following we will present results for an abort at 0 seconds after the drop off, i.e., for the case when the engine does not ignite. This is the worst case scenario in which the engine does not start and the vehicle needs to be recovered. This also corresponds to having only 2 conceptual phases, but the simulations were carried out using 3 phases, where phase 3 was matched to the beginning of phase 1 instead of its end.

The problem was discretised with 3 elements per phase, using Bernstein polynomials of order 7 for all states and controls. MACS was run with standard settings and 20000 function evaluations (corresponding to about 1.5 hr run time). The abort manoeuvre was constrained to terminate at 2 km altitude, $M = 0.4$ and $\gamma_f \geq -10$ deg.

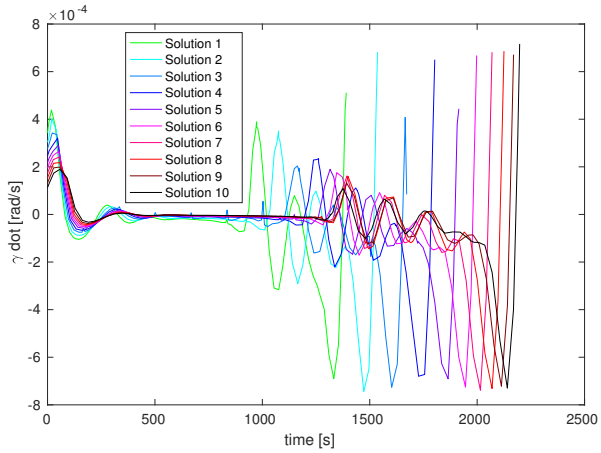

(a) Flight path angle differential $\dot{\gamma}$

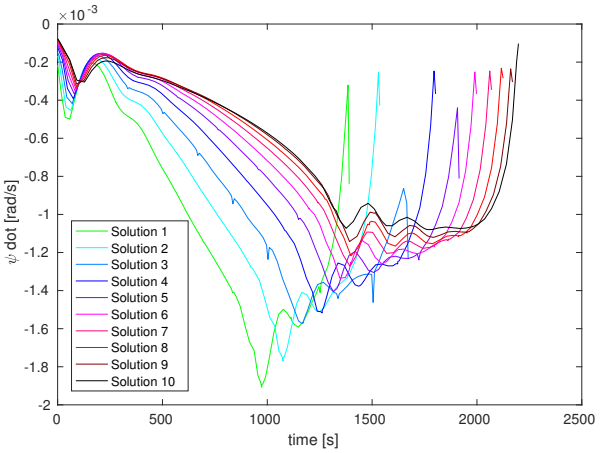

(b) Azimuth angle differential $\dot{\psi}$

Fig. 9 Time-history of the rate of change of the flight path $\dot{\gamma}$ and azimuth $\dot{\psi}$ angles for each of the 10 solutions shown on the Pareto front

The corresponding Pareto front is reported in Fig. 10a. The solution is well spread and the Pascoletti-Serafini scalar problems are solved down to an accuracy of 10^{-6} in both optimality and feasibility. The associated wing loading and downrange for all the solutions in the Pareto front are shown in Fig. 10b. Note that the archive of Pareto optimal solutions in MACS was set to 10 elements, therefore, the Pareto front is here formed only by 10 solutions.

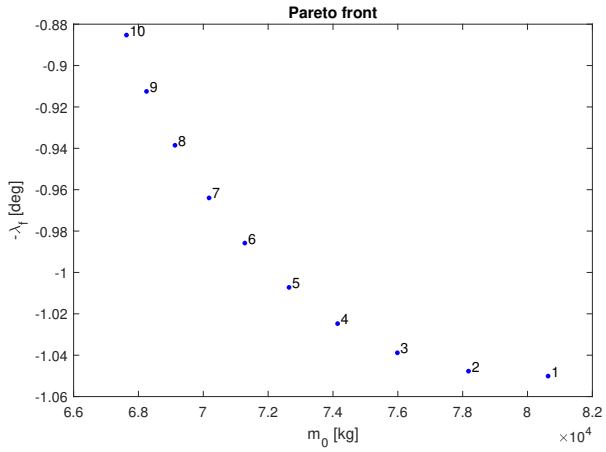

(a) Pareto front for the 0 s abort scenario

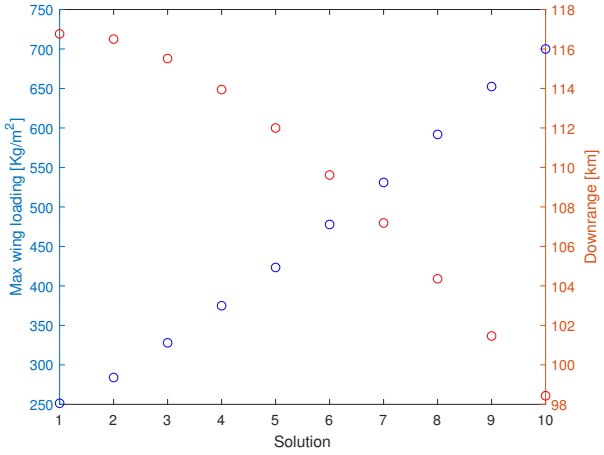

(b) Wing loading and downrange for the 0 s abort scenario

Fig. 10 Pareto front and wing loading vs downrange for each solution of an abort at 0 seconds.

For this case the ascent and abort trajectories do not significantly affect each other given that the abort phase starts at the beginning of the ascent. The main trade-off is on the type of vehicle as the wing loading changes from one solution to the other and, as a consequence, the overall aerodynamics. This is reflected also in the flight path angle and is very pronounced in the case of the solution 1 which corresponds to the maximum downrange. However, the two branches are not coupled only by the aerodynamic surface but also by the initial mass, angle of attack and flight path angle, which affect both trajectory legs, thus the abort trajectory is indirectly influenced by the ascent trajectory and vice versa.

The wing area seems to be the main driver of the trade-off, and is bounded from below by the maximum allowable wing loading, which reaches the maximum value of 700 kg/m^2. High downrange solutions prefer larger wing areas which impose a penalty in initial mass both because of the higher drag and because of the higher mass of the wings themselves. However, the relative increase in wing area, and hence mass, with respect to initial vehicle mass is such that

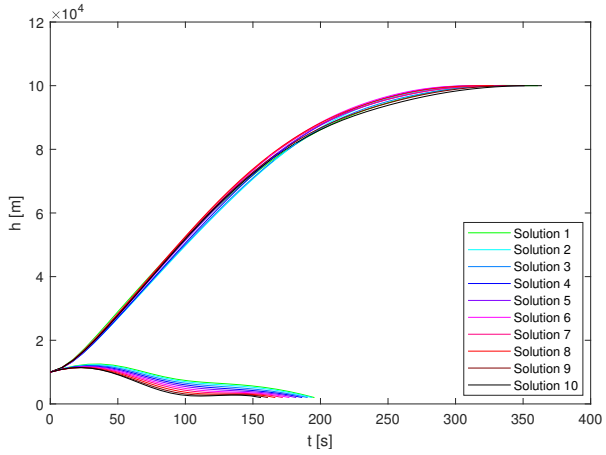

(a) Altitude time history

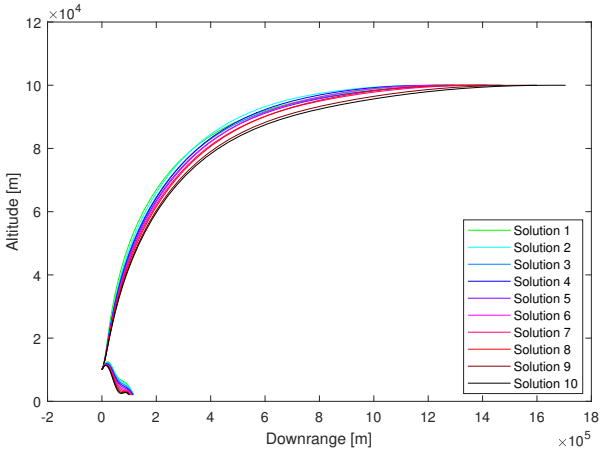

(b) Altitude vs downrange

Fig. 11 Time history of altitude and altitude vs downrange for an abort at 0 seconds.

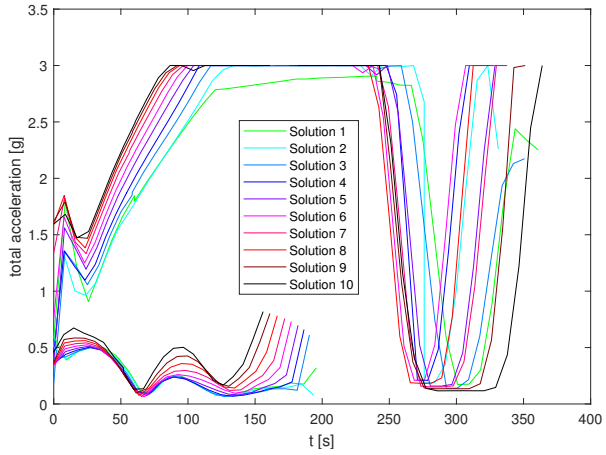

(a) Total acceleration time history

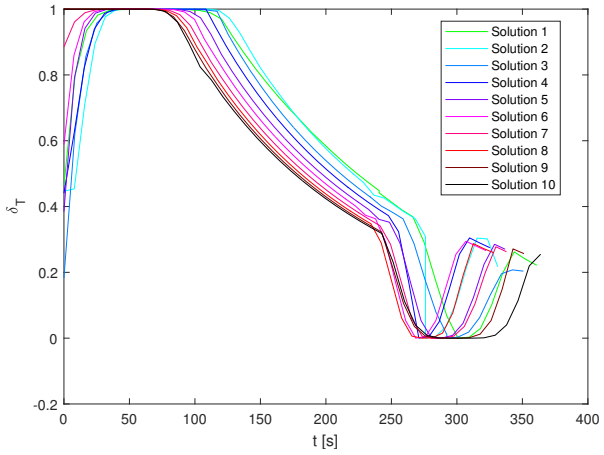

(b) Throttle time history

Fig. 12 Time histories for total acceleration and engine throttling for an abort at 0 seconds.

wing loading actually decreases. Thus, solutions with larger wings have an overall lower wing loading and are able to generate larger downrange abort trajectories.

Figure 11 shows the ascent and abort trajectory profiles over time and over downrange. Figure 12a shows the time history of the total acceleration experienced by the vehicle. All ascent phases are characterised by a maximum acceleration region in approximately the same time interval. This is echoed in the throttle profile shown in Figure 12b. For the first minute, the throttle is at the maximum value. High downrange solutions however seem to delay the maximum throttle segment. After that, the throttle is progressively reduced to comply with the limits on the accelerations. It is worth noting that even when the throttle assumes the maximum value for a finite time interval, no oscillations or crossing of the boundaries can be observed, thanks to the use of Bernstein polynomials. Different basis functions would have resulted in highly oscillating solutions, even crossing the bounds for the controls.

Overall, the solutions seem to form a compact family of trajectories: the ascent and abort profiles look quite similar, with the main difference being the slightly noisier acceleration profile in the ascent phase. This is likely motivated by the fact that the optimiser is only looking at maximising the downrange, and thus no optimisation is performed on the ascent, it simply suffices that the constraints are met. It might be possible that there exists a solution with the same downrange but with a better initial mass, which would thus dominate the current minimum downrange solution.

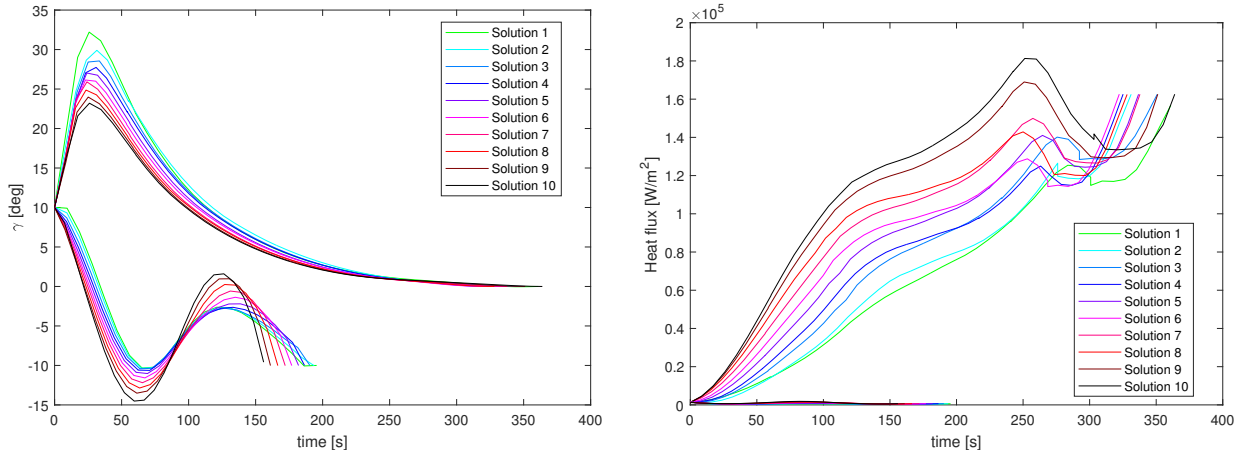

(a) Flight path angle γ time history

(b) Heat flux time history

Fig. 13 Time histories of flight path angle and heat flux for an abort at 0 seconds.

However, the algorithm was not able to find such a solution in the given computational budget. A pure single objective optimisation of the initial mass was also unable to find a better result.

VI. Conclusion

This paper presented a novel approach to the solution of multi-phase, multi-objective optimal control problems applied to the ascent, re-entry and abort descent cases for different hypothetical spaceplanes. The approach, combining DFET with MACS and using a novel parametrisation of the controls based on Bernstein polynomials provides a reliable method to compute sets of Pareto optimal solutions. In particular the smooth transition from Chebyshev to Pascoletti-Serafini scalarisation allows for an effective local refinement of the solutions and a global exploration of the search space.

It was also shown that the use of Bernstein bases, for the transcription of the controls, ensures that the upper and lower bounds are respected throughout the trajectory, not just at the control nodes. At the same time the sparsity of the Jacobian matrix is similar to previous DFET transcriptions. The approach was validated on a known case from the literature confirming the ability to reconstruct a well converged Pareto front with a good spreading of the solutions.

The abort scenario contemplated the worst case in which the engine does not start and the vehicle needs to be recovered after drop-off. In this case the trade-off on the wing loading affects the ascent trajectory as the aerodynamics of the vehicle changes due to the need to improve flight performance during descent. Future work will consider additional abort scenarios.

Appendix

Table 1 reports the coefficients used for the aerodynamic model in Section C.

Acknowledgments

The research was partially funded by an ESA NPI grant (ref TEC-ECN-SoW-20140806) and Airbus Defence & Space.

References

[1] Vasile, M., "Finite Elements in Time: A Direct Transcription Method for Optimal Control Problems," *AIAA/AAS Astrodynamics Specialist Conference*, 2010.

[2] Ricciardi, L. A., and Vasile, M., "Improved archiving and search strategies for Multi Agent Collaborative Search," *International*

Table 1 Coefficients for the aerodynamic model

Coeff.	Value	Coeff.	Value	Coeff.	Value
$a_{1,0}$	-6.378335936032101e-02	λ_1	1.344774373794846e+00	$a_{5,3}$	-1.683702441539749e-04
$a_{1,1}$	1.976923220591986e-02	λ_2	1.542614382500486e+00	$a_{6,0}$	8.869412111210242e+00
$a_{1,2}$	2.973963976446931e-04	s_1	-3.100574615791786e+01	$a_{6,1}$	7.482402265848023e-01
$a_{2,0}$	-3.349264465313049e+05	s_2	-9.123166455265215e-02	$a_{6,2}$	2.604898066115986e-02
$a_{2,1}$	6.001178833841350e+05	$a_{4,0}$	4.941304084167961e-02	$a_{6,3}$	2.689898581212407e-04
$a_{2,2}$	-2.862064269172794e+04	$a_{4,1}$	-2.771101541363621e-03	k_3	1.348770573128532e+00
$a_{3,0}$	4.398289382706495e-01	$a_{4,2}$	4.195518696508440e-04	k_4	1.376496163657956e+00
$a_{3,1}$	6.555024080116524e-02	$a_{4,3}$	6.144719928912810e-06	λ_3	1.004292397340135e+00
$a_{3,2}$	-4.816546419307238e-04	$a_{5,0}$	-8.408713897701869e+00	λ_4	1.053245533842992e+00
k_1	1.088199979257513e+00	$a_{5,1}$	-6.942588805953275e-01	s_3	-2.715562764314760e-01
k_2	1.523372394108941e+00	$a_{5,2}$	-2.602381527566895e-02	s_4	-3.464086848960685e-01

Conference on Evolutionary and Deterministic Methods for Design, Optimization and Control with Applications to Industrial and Societal Problems (EUROGEN), 2015.

[3] Vasile, M., and Finzi, A. E., "Direct lunar descent optimisation by finite elements in time approach," *International Journal of Mechanics and Control*, Vol. 1, No. 1, 2000.

[4] Vasile, M., and Bernelli-Zazzera, F., "Optimizing low-thrust and gravity assist maneuvers to design interplanetary trajectories," *Journal of the Astronautical Sciences*, Vol. 51, No. arXiv: 1105.1829, 2011, pp. 13–35.

[5] Vasile, M., and Bernelli-Zazzera, F., "Targeting a heliocentric orbit combining low-thrust propulsion and gravity assist manoeuvres," *Operational Research in Space & Air*, Vol. 79, 2003.

[6] Bottasso, C. L., and Ragazzi, A., "Finite element and runge-kutta methods for boundary-value and optimal control problems," *Journal of Guidance, Control, and Dynamics*, Vol. 23, No. 4, 2000, pp. 749–751.

[7] Ricciardi, L. A., Vasile, M., Toso, F., and Maddock, C. A., "Multi-Objective Optimal Control of the Ascent Trajectories of Launch Vehicles," *AIAA/AAS Astrodynamics Specialist Conference*, 2016, p. 5669.

[8] Goddard, R. H., "A Method of Reaching Extreme Altitudes," *Nature*, Vol. 105, 1920, pp. 809–811.

[9] Munick, H., "Goddard problem with bounded thrust," *AIAA Journal*, Vol. 3, No. 7, 1965, pp. 1283–1285.

[10] Tsiotras, P., and Kelley, H. J., "Goddard problem with constrained time of flight," *Journal of guidance, control, and dynamics*, Vol. 15, No. 2, 1992, pp. 289–296.

[11] Seywald, H., and Cliff, E. M., "Goddard problem in presence of a dynamic pressure limit," *Journal of Guidance, Control, and Dynamics*, Vol. 16, No. 4, 1993, pp. 776–781.

[12] Graichen, K., and Petit, N., "Solving the Goddard problem with thrust and dynamic pressure constraints using saturation functions," *World Congress of The International Federation of Automatic Control, IFAC World Congress*, 2008.

[13] Pagano, A., and Mooij, E., *Global launcher trajectory optimization for lunar base settlement*, American Institute of Aeronautics and Astronautics (AIAA), 2010.

[14] Toso, F., and Maddock, C., "Return and abort trajectory optimisation for reusable launch vehicles," *AIAA/IAA International Space Planes and Hypersonic Systems and Technologies Conferences*, 2017.

[15] Betts, J. T., *Practical methods for optimal control and estimation using nonlinear programming*, SIAM, 2010.

[16] Rizvi, S., He, L.-S., and Xu, D.-J., "Optimal trajectory and heat load analysis of different shape lifting reentry vehicles for medium range application," *Defence Technology*, Vol. 11, No. 4, 2015, pp. 350 – 361.

[17] Pamadi, B. N., and Brauckmann, G. J., "Aerodynamic characteristics and development of the aerodynamic database of the X-34 reusable launch vehicle," *International Symposium on Atmospheric Reentry Vehicles and Systems*, 1999.

[18] Rohrschneider, R., "Development of a mass estimating relationship database for launch vehicle conceptual design," *AE8900 Special Project, School of Aerospace Engineering, Georgia Institute of Technology*, 2002.

[19] Hodges, D. H., and Bless, R. R., "Weak Hamiltonian finite element method for optimal control problems," *Journal of Guidance, Control, and Dynamics*, Vol. 14, No. 1, 1991, pp. 148–156.

[20] Ricciardi, L. A., and Vasile, M., "Global Solution of Multi-objective Optimal Control Problems with Multi Agent Collaborative Search and Direct Finite Elements Transcription," *IEEE World Congress on Computational Intelligence, IEEE Congress on Evolutionary Computation*, 2016.

[21] Vasile, M., and Ricciardi, L., "A direct memetic approach to the solution of Multi-Objective Optimal Control Problems," *Computational Intelligence (SSCI), 2016 IEEE Symposium Series on*, IEEE, 2016, pp. 1–8.

[22] Ghomanjani, F., Farahi, M. H., and Gachpazan, M., "Bézier control points method to solve constrained quadratic optimal control of time varying linear systems," *Computational & Applied Mathematics*, Vol. 31, No. 3, 2012, pp. 433–456.

[23] Ghomanjani, F., and Farahi, M. H., "Optimal control of switched systems based on Bezier control points," *International Journal of Intelligent Systems and Applications*, Vol. 4, No. 7, 2012, p. 16.

[24] Rogalsky, T., "Bézier parameterization for optimal control by differential evolution," *International Conference on Genetic and Evolutionary Methods*, 2011, pp. 28–34.

[25] Kano, H., Egerstedt, M., Nakata, H., and Martin, C. F., "B-splines and control theory," *Applied mathematics and computation*, Vol. 145, No. 2, 2003, pp. 263–288.

[26] Darehmiraki, M., Farahi, M. H., and Effati, S., "A Novel Method to Solve a Class of Distributed Optimal Control Problems Using Bezier Curves," *Journal of Computational and Nonlinear Dynamics*, Vol. 11, No. 6, 2016.

[27] Zuiani, F., Kawakatsu, Y., and Vasile, M., "Multi-objective optimisation of many-revolution, low-thrust orbit raising for destiny mission," *23rd AAS/AIAA Space Flight Mechanics Conference*, 2013.

[28] Eichfelder, G., *Adaptive Scalarization Methods in Multiobjective Optimization*, Springer-Verlag Berlin Heidelberg, 2008.